AIAA JOURNAL
Vol. 39, No. 5, May 2001

Characteristics of the Compressible Shear Layer over a Cavity

Robert C. Murray* and Gregory S. Elliott†
Rutgers University, Piscataway, New Jersey 08854

The compressible shear layer over a 3:1 rectangular cavity was investigated using schlieren photography and planer laser imaging at freestream Mach numbers of 1.8, 2.1, 2.8, and 3.5. The purpose of this investigation was to study the characteristics of the shear layer structures and their convective velocity over this Mach number range. Schlieren images show leading- and trailing-edge shock waves, as well as shock waves emanating from the shear layer, which became less prevalent as the Mach number increased. Streamwise planar laser sheet lighting images indicate the existence of organized roller-type structures at the lower Mach numbers studied ($M = 2.1$ and 2.8). These structures became less coherent as the Mach number was increased, although the cavity appears to cause the large-scale structures to persist at higher levels of compressibility than found in planar free shear layers. Plan view images indicate that the two dimensionality of the large-scale structures decreased with increasing Mach number. Autocorrelations performed on single-pulse images show that the structure size decreased 63% when the freestream Mach number was increased from 1.8 to 3.5. By double pulsing the laser at delays of 15, 20, and 25 μs, the evolution of the large-scale structures were investigated and quantified. The correlations were found to decrease by 23% for the same nondimensional time when increasing the Mach number from 2.1 to 3.5. From the shift of the peak correlation, the convective velocity was calculated for each case and found to vary laterally across the shear layer. At a lateral location most representative of the large-scale structures in the shear layer, the variation in convective velocity with Mach number was best represented by 0.57 times the freestream velocity.

Introduction

CAVITIES have long been an important research topic due to their interest as a fundamental fluid dynamic phenomenon, as well as simulating practical applications on aircraft such as store release and wheel wells.[1] The use of cavities in supersonic flows has also been investigated in areas such as flame holding and fuel/air mixing arrangements in proposed scramjet engines and flow control of supersonic nozzles and jets.[2] Figure 1 gives a schematic of the basic two-dimensional cavity studied in the present investigation. The cavity flowfield is quite complex, consisting of three regions of interest: the external freestream, shear layer, and flowfield within the cavity. Also, the cavity flowfield may exhibit a variety of flow characteristics. For example, the cavity flowfield may exhibit either fluid dynamic (where the primary mechanism of excitation is the amplification of unstable disturbances in the shear layer) or fluid resonant (characterized by a resonant standing wave in the cavity that governs the characteristics of the oscillation) oscillations.[3] Furthermore, the oscillations may have either transverse (normal to the streamwise direction) or longitudinal (parallel to the streamwise direction) orientations. For $L/D > 10$, the shear layer will usually attach to the floor (defined as a closed cavity), whereas for $L/D < 10$, the shear layer will usually span the cavity (defined as an open cavity).[4]

A major concern in store release applications is the streamwise oscillation in shallow cavities.[5] Several similar, but distinct, mechanisms of longitudinal oscillation have been proposed. One of the first was by Rossiter,[6] who proposed that a shear layer structure impinging on the trailing edge of a cavity would cause a pressure wave to travel upstream through the cavity at the local speed of sound (which was assumed to be the same as the freestream speed of sound). The pressure wave would then be traveling at a supersonic rate with respect to the freestream and be trailed by a shock in the freestream. When the pressure wave reaches the leading edge, it causes another shear layer structure to roll off. This structure is then convected downstream at some convective velocity U_c. This shear layer structure causes another pressure wave at the trailing edge, which completes the cycle. To nondimensionalize the frequency, Rossiter defined a Strouhal number based on cavity length and the freestream velocity:

$$Sr_m = \frac{f_m L}{U_e} = \frac{m - \alpha}{1/k_c + M_e} \tag{1}$$

where f_m and m are the frequency and mode of the oscillation, M_e is the freestream Mach number, and k_c is the ratio of the convective velocity of the vortical structures in the shear layer to the freestream velocity (U_c/U_e). Here, α is the phase delay between the interaction of the pressure wave with the leading edge and the subsequent formation of a new shear layer structure. With curve fits and experimental data, α and k_c were found to be 0.25 and 0.57, respectively, but these values are still debated. Heller and Bliss[7] have modified Rossiter's[6] formula to account for temperature recovery within the cavity. Although the frequency and mode of oscillation can be predicted by Rossiter's[6] modified formula, there still remains no simple means of determining which modes will dominate and what their amplitude will be.[7,8]

Experimental evidence of flow over open cavities shows shear layer structures convecting downstream from the leading edge, as well as vertical oscillations of the shear layer. In a study of drag on shallow cavities, McGregor and White[9] used a high-frequency schlieren system, capable of taking 9000 images per second, to image the flowfield over a cavity. Although the flow was subsonic ($M = 0.555$ and $L/D = 2$), a steady train of vortical structures were clearly seen to be convecting downstream from the leading edge. Zhang and Edwards[10] have found similar results at Mach 1.5 and 2.5 using both experiment and numerical solution of the Navier–Stokes equations. In their work, Zhang and Edwards report that a steady train of vortical structures (also termed large-scale structures) in the shear layer are convected downstream of the leading edge and interact with the trailing edge (Fig. 1). Although the convective velocity of the vortical structure is, in general, taken to be constant ($0.57U_e$), Zhang and Edwards[10,11] suggest that the speed of the vortex shed from the leading edge of the cavity is not constant at supersonic speeds.

Similar to cavities, compressible planar free shear layers have been studied for many years. The research was originally motivated by the observed decrease in the growth rate of the shear layer for the

Received 22 June 1999; revision received 4 October 2000; accepted for publication 6 October 2000.

*Graduate Student, Department of Mechanical and Aerospace Engineering. Student Member AIAA.

†Associate Professor, Department of Mechanical and Aerospace Engineering. Member AIAA.

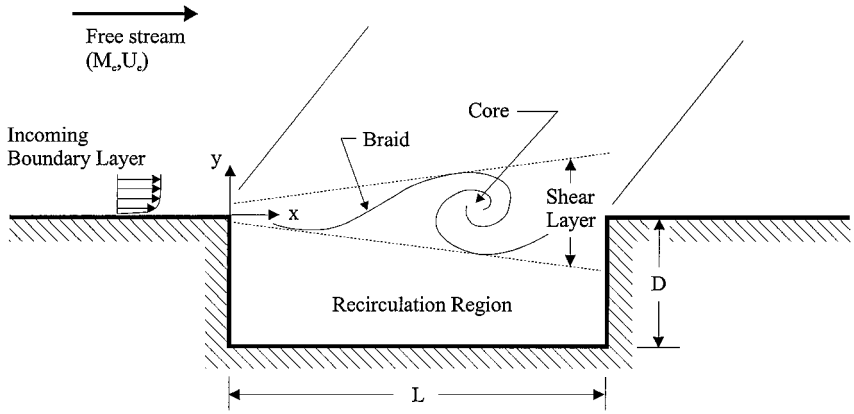

Fig. 1 Schematic of compressible two-dimensional cavity flowfield.

supersonic case. Papamoschou and Roshko[12] demonstrated that the observed decrease in growth rate was due to compressibility effects and correlated the trend to a parameter termed the convective Mach number M_c. The convective Mach number is a Mach number of a frame of reference traveling with the large-scale structures in the shear layer, which, for a planar free shear layer, is given as

$$M_c = (U_1 - U_c)/a_1 = M_1(1 - k_c) \tag{2}$$

and the convective velocity U_c is given by

$$U_c = \frac{a_1 U_2 + a_2 U_1}{a_1 + a_2} \tag{3}$$

where U_1 and U_2 are the velocities of the high- and low-speed streams, respectively, and a_1 and a_2 are the speeds of sound of the two streams. Note that, recently, investigators have modified the convective Mach number to take into account recompression shocks that may be present within the shear layer at high compressibility levels.[13,14] Other investigators have shown that the convective Mach number also correlates trends in the turbulence profiles and shear layer characteristics.[15,16] Also, the convective Mach number describes trends in the large-scale structures, which have been found in compressible shear layers. At moderate convective Mach numbers, these structures have well-defined core and braid regions similar to those described by Brown and Roshko[17] for incompressible shear layers as illustrated in Fig. 1. As the convective Mach number increases, large-scale structures have been reported to be less coherent and more three-dimensional in planar free shear layers.[18–20]

With Eq. (3), the convective velocity of the shear layer over a cavity can be determined as an alternative to the value of $k_c = 0.57$, used by other investigators. Rossiter[6] and Heller and Bliss,[7] by their assumption that the pressure wave in the cavity travels upstream at the local speed of sound, imply that the velocity of the fluid in the cavity is negligible. They also assume an adiabatic temperature recovery by setting the temperature of fluid in the cavity to be equal to the stagnation temperature. If we take Eq. (3) to be a valid measure of the convective velocity, the convective velocity ratio for the cavity flow can be given by

$$k_c = \frac{1}{a_1/a_2 + 1} = \left\{ \frac{1}{\sqrt{1 + [(\gamma - 1)/2]M_e^2}} + 1 \right\}^{-1} \tag{4}$$

In the current investigation the two theoretical equations for k_c will be compared to experimental results.

Cavities have been studied previously using a variety of experimental techniques including hot wires, pressure measurements[21] (both average and at high frequency), interferometry,[10] schlieren photography,[9] and planar laser sheet flow visualizations.[22] Although much insight into the flowfield can be gained from these techniques, there is still a need to describe the properties of the shear layer formed above these cavities.

Table 1 Flow properties at the Mach numbers investigated

	Stagnation conditions		Freestream conditions		Shear layer predictions from Eqs. (2) and (4)	
M	T_{stag}, K	P_{stag}, kPa	U_1, m/s	$Re_L/10^6$	k_c	M_c
1.8	280	220	470	1.4	0.56	0.79
2.1	280	344	513	1.8	0.58	0.88
2.8	280	724	586	2.8	0.62	1.08
3.5	280	1000	632	2.6	0.65	1.22

Experimental Setup

Experiments were performed at the Rutgers University Gasdynamics and Laser Diagnostics Laboratory utilizing a variable Mach number blowdown wind tunnel. A full description of the tunnel is found in Ref. 23. The test section has a rectangular cross section measuring 101.6 mm wide × 114.3 mm high. The Mach number of the tunnel may be varied by means of a sliding nozzle block. The tunnel is able to operate with good flow quality (absence of strong compression or expansion waves in the test section) from approximately Mach 1.8 to 3.5. Compressed air is supplied by two Ingersoll Rand Model 15T4 four-stage air compressors. The compressed air is then passed through two trap filters that remove oil and residual water followed by a Baur Secant III regenerative high-pressure air dryer.

Seeding for flow visualizations used an ethanol reservoir that was pressurized with nitrogen to drive the ethanol into the tunnel supply pipe after the pressure control valve. The ethanol injected through the seeding nozzle evaporates as it passes through the pipe and stagnation chamber and subsequently condenses to form small particles as the temperature drops through the converging/diverging nozzle. This type of seeding was termed passive scalar formation by Clemens and Mungal.[18] The relatively slower, and, therefore, warmer fluid in the boundary layer and cavity prohibits condensation, resulting in dark regions in the flow when illuminated by a laser sheet. Bright regions mark the colder supersonic fluid. Based on previous studies using similar seeding techniques, the particle size was estimated to be on the order of 50 nm (Ref. 15). Previous work by Samimy and Lele[24] has found that these particles will accurately track the large-scale turbulent structures pertinent in this investigation.

Four Mach numbers ranging from the lowest to the highest Mach number attainable in the supersonic wind tunnel were used in the current investigation. Flow conditions including the Mach number, stagnation pressure and temperature, freestream velocity, Reynolds number based on the cavity length, and convective velocity and Mach number calculated from Eqs. (2) and (4) are given in Table 1. The dimensions of the cavity used in the present study were 12.7 mm deep × 38.1 mm long. The cavity spanned across the width of the wind tunnel; therefore, note that the undisturbed core is reduced by the side wall boundary layers. The depth of the cavity was limited by the thickness of the wind-tunnel wall section containing the cavity.

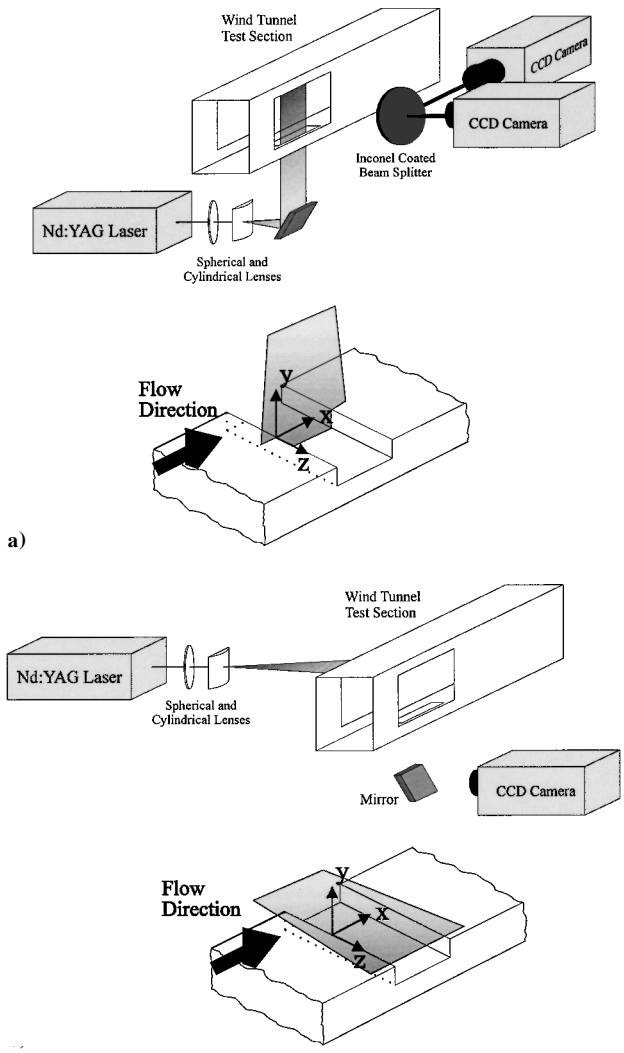

Fig. 2 Basic geometries used to image the flow showing the experimental setup for a) streamwise imaging and b) plan view imaging.

To visualize the flowfield, a laser sheet was formed using a combination of spherical and cylindrical optics providing streamwise (Fig. 2a) and plan (Fig. 2b) views of the flow. The laser used in these experiments was a Spectra Physics GCR-230 Nd:YAG pulsed laser. The frequency-doubled beam has a maximum output of approximately 600 mJ per pulse at a wavelength of 532.8 nm. The duration of the pulse is on the order of 10 ns, resulting in relatively instantaneous visualizations. By multiple Q switching, the Nd:YAG laser can be double pulsed with time delays ranging from 15 to 200 μs. For this investigation, time delays of 15, 20, and 25 μs were used to study the evolution of the structures above the cavity.

Images were recorded on two Princeton Instruments 14-bit intensified charge-coupled device (CCD) cameras. A $\frac{50}{50}$ Inconel beam splitter was placed between the two cameras, which were adjusted so that they had identical views. Images were taken, stored, and processed using Pentium® 100-MHz personal computers. The computers also provided camera control and laser synchronization. In all cases, the cavity was on the ceiling of the tunnel, but for ease of comparison with other studies, images were flipped vertically showing the cavity to be on the bottom of the image.

Instantaneous schlieren images were taken with a system set up in the Z arrangement using two parabolic mirrors, each having a 9-ft focal length. A video camera was used to record the schlieren images, which were later digitized on a personal computer.

Incoming Boundary Layer

Measurements were made to determine the characteristics and state of the incoming boundary layer, which are summarized in Table 2. Boundary-layer data were obtained by traversing a pitot probe from the tunnel wall into the freestream, and the Mach number and mean velocity profile were determined similar to other studies of compressible turbulent boundary layers.[25] There is a general agreement among researchers that the Van Driest compressibility transformation coupled with the wall–wake law of Coles is a successful scheme for correlating the similarity of compressible boundary layer profiles (see Ref. 26). From the friction velocity and wall temperature, the empirical values of the coefficient of skin friction $C_{f,\text{empirical}}$ can be calculated and are given in Table 2 (details of this analysis for the present experiment can be found in Ref. 23). To determine whether the turbulent boundary layer was fully developed, these empirical values of skin friction $C_{f,\text{empirical}}$ were compared to values of skin friction predicted using a procedure described by Hopkins and Inouye,[27] which are given in Table 2 as $C_{f,\text{Van DriestII}}$. The empirically determined values of C_f were found to have the same order as those predicted by Van Driest II. For the Mach 2.1, 2.8, and 3.5 cases, C_f is within the measurement uncertainty and 10% criteria suggested by Ref. 27 for fully developed turbulent boundary layers. The higher three Mach number cases are, therefore, assumed to have equilibrium turbulent boundary layers. The Mach 1.8 case, however, does not perfectly fit predicted values and, therefore, it may not be fully developed.

Table 2 Properties of the incoming boundary layer

M	δ, mm	θ, mm	$Re_\theta/10^4$	$C_{f,\text{Van DriestII}}$	$C_{f,\text{empirical}}$
1.8	13.0	1.8	6.7	0.0022	0.0014
2.1	14.3	1.8	8.4	0.0018	0.0016
2.8	15.0	2.3	16.5	0.0011	0.0011
3.5	17.5	2.9	19.7	0.00085	0.00097

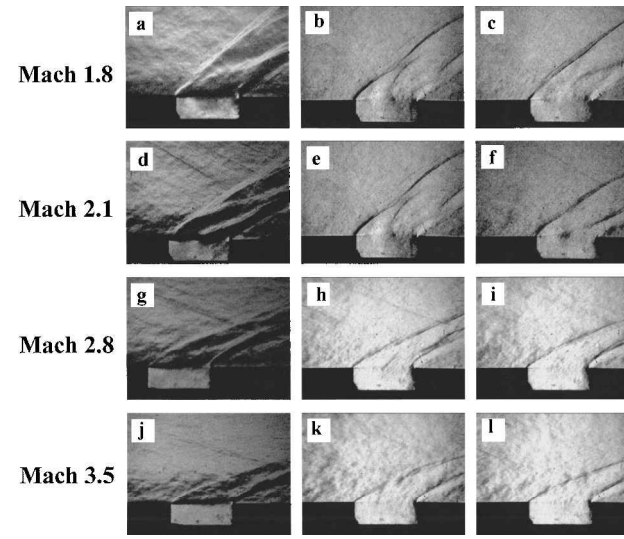

Fig. 3 Schlieren images of flow over the cavity taken with a, d, g, j) horizontal and b, c, e, f, h, i, k, l) vertical a, d, g, j) knife edge.

Results

Schlieren Images

Schlieren images of flow over the cavity were taken using a horizontal knife edge and a vertical knife edge (Fig. 3). In each case, the images were chosen to show key aspects of the flowfield and are therefore, not related in time. In the schlieren images taken with a horizontal razor blade (Figs. 3a, 3d, 3g, and 3j), vertical density gradients due to the boundary layer and the shear layer, as well as shock waves, are clearly visible. It is also clear that whereas their exact form and intensity may vary, the leading- and trailing-edge shocks are consistently seen in the flowfield. Furthermore, at least at the lower three Mach numbers, a shock is intermittently observed emanating from the shear layer. Whereas these shocks are seen in nearly all of the images at Mach 1.8 and 2.1, in many, if not most

of the frames at Mach 2.8 and nearly all of the images at Mach 3.5, the fluctuating shock is absent.

In Fig. 3, with the knife-edge orientated vertically (panels b, c, e, f, h, i, k, and l), the vertical density gradients due to the shear layer and the boundary layer are more suppressed in the images. The advantage of this setup is that it allows large-scale structures within the shear layer to be more easily visualized. Figures 3b, 3c, 3e, 3f, and 3h show such a shear layer structure and the apparent relationship between the shear layer structure and the fluctuating shock over the cavity. Again, these shear layer structures are either too weak to be seen, less coherent, more three dimensional, or nonexistent at Mach 2.8 and 3.5 (this point will be clarified in the planar imaging sections to follow). Similar large-scale (or vortical) structures were first recorded and reported over subsonic cavities by McGregor and White in 1970 (Ref. 9) and are also observed in interferograms by Zhang and Edwards[10] and in computational models[5] for the compressible case.

The exact relationship between the shock and the structures in the shear layer is not clear from the schlieren. At times the shock appears to emanate from the shear layer structure at a normal angle (Figs. 3b, 3c, 3e, and 3h), and at other times it emanates at an oblique angle (Figs. 3f and 3h). There are two plausible explanations given in the literature for the source of these shock waves; one from investigations of supersonic cavities[3,5,22] and the second from investigations of compressible shear layers.[13,14] As described by Rizzetta,[5] pressure waves propagate in the cavity and, when reflected from the aft wall, propagate upstream at supersonic speeds relative to the external freestream. This produces a compression wave in the freestream external to the cavity.[5] A second possibility is that the shock wave emanates from the large-scale structures in the shear layer, which has been suggested by Unalmis et al.[22] From studies of compressible shear layers, when the convective Mach number is greater than one, recent investigations have found shocklets to emanate from large-scale structures in the shear layer.[13,14] This would also result in the shock wave traveling downstream with the large-scale structures in the shear layer. Heller and Delfs[28] and Zhang et al.[29] have shown that the angle of the waves depends on the direction and speed of the large-scale structures. For large-scale structures traveling downstream, the relative Mach number will be small and the resulting Mach angle of the wave emanating from it will be relatively large. When structures or perturbations in the cavity travel upstream (i.e., as a large-scale structure interacts with the back wall causing an upstream traveling pressure wave in the cavity) the relative Mach number of the perturbation is greater, and, therefore, the Mach angle of the resulting wave is small. These observations are confirmed in the schlieren images shown.

Planar Laser Images

All planar laser images presented here have been processed to remove laser intensity fluctuations, background scattering, and intensity variations across the laser sheet due to the Gaussian profile of the laser beam.[23] To analyze the evolution of the large-scale structures in the following image analysis, correlation techniques were utilized. These techniques are an excellent method for characterizing the evolution of large-scale structures within a shear layer and for calculating their convective velocities.[19,30–32] To do this, a window is selected within the initial image of an image pair. This window (which will be referred to as the initial correlation window) should presumably contain some flow structure or variation. The initial window is then correlated with corresponding windows at various spatial offsets in the delayed image according to the following correlation function:

$$R(\delta x, \delta y) = \frac{\sum_{i,j}\{[f(i,j) - \bar{f}(0,0)][g(i+\delta x, j+\delta y) - \bar{g}(\delta x, \delta y)]\}}{\sqrt{\sum_{i,j}[f(i,j) - \bar{f}(0,0)]^2 \sum_{i,j}[g(i+\delta x, j+\delta y) - \bar{g}(\delta x, \delta y)]^2}} \tag{5}$$

where f and g refer to the fluctuating pixel intensities (the averaged image is subtracted) in the initial and delayed images, respectively. The subscripts i and j span the initial correlation window; $\bar{f}(\delta x, \delta y)$ and $\bar{g}(\delta x, \delta y)$ refer to the spatial average of the window spanned by i and j at the $\delta x, \delta y$ offset. The $\delta x, \delta y$ offset of the peak correlation should then correspond to how far the structures in the initial correlation window have moved during the time delay between the images. The correlation coefficient R varies between 1 (if g is a positive scalar multiple of f) and -1 (if g is a negative scalar multiple of f). A full description of the correlation function along with algorithms by which it may be efficiently calculated are given in Ref. 23. Sets of 375 images were recorded at each Mach number and time delay to calculate the statistics of the flow with an uncertatinty within 5% (Ref. 19).

Streamwise View Images

Figure 4 gives four sets of three instantaneous streamwise view (x–y) images taken at each of the Mach numbers studied. The flow is moving from left to right with the physical cavity starting at $x/D = 0$. The cavity is outlined in white. The first characteristic that is observed in the instantaneous images is the presence of

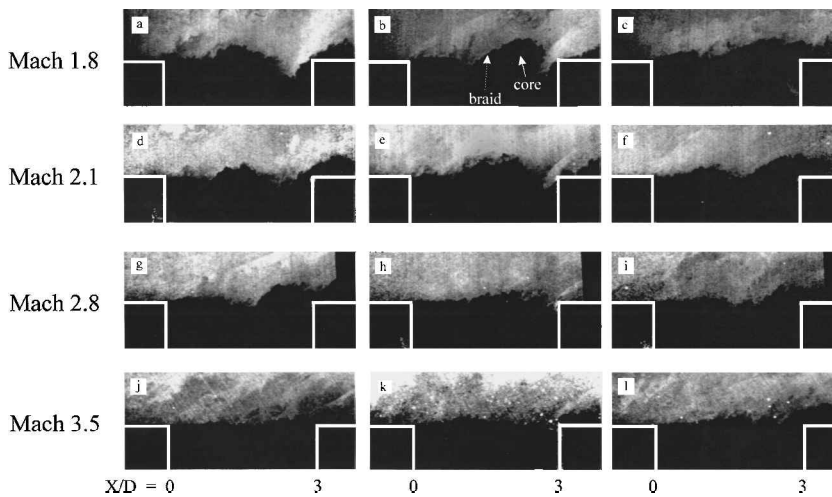

Fig. 4 Single-pulse streamwise images. The flow is moving from left to right, with the physical cavity outlined in white. The core and braid regions of a roller-type structure are marked in image b.

well-defined roller-type structures (also termed vortical structures) for the lower two Mach numbers (1.8 and 2.1). These large-scale structures have distinct core and braid regions (marked in Fig. 4b) as defined by Brown and Roshko[17] for subsonic planar free shear layers and observed in some compressible free shear layers[18–20] These large-scale structures have been determined to be a major contributor to the turbulence in the shear layer as well as crucial to mixing.

It is quite evident that the scale and coherence of the large-scale structures is greatly reduced as the freestream Mach number is increased. A similar phenomenon has been observed in planar free shear layers where the coherence, size, and two dimensionality of large-scale structures has been found to decrease with increasing convective Mach number.[18–20] Note in Fig. 4 that as the freestream Mach number increases there is a decrease in scale and organization of the large-scale structures. In general, this decrease in scale and organization is reported to take place for planar mixing layers at a convective Mach number of approximately 0.6 (Refs. 18–20) In the present experiments of the shear layer over a cavity, this transition appears to begin near Mach 2.8 (corresponding to $M_c \approx 1.08$). This suggests that the cavity, and subsequent oscillation, enhances the formation of structures in the shear layer.

The images shown in Fig. 4 are not related in time and were selected to show three characteristics of the large-scale structures present in the shear layer. For each of the Mach numbers, the first image (Figs. 4a, 4d, 4g, and 4j) shows a structure extending into the cavity and traveling toward the trailing edge. The second image (Figs. 4b, 4e, 4h, and 4k) in each set shows the shear layer impinging on the trailing edge of the cavity along with the associated shock. The third image of each set (Figs. 4c, 4f, 4i, and 4l) shows mass ejection after a structure has impinged on the trailing edge of the cavity, and, for the Mach 1.8 and 2.1 flow, remains of a large-scale structure appear to be left in the cavity near the trailing edge. When the shear layer is deflected over the trailing edge, for example, Figs. 4c and 4g, it appears that the trailing-edge shock is weakened. The unsteady impingement of the large-scale structure on the trailing edge and subsequent formation of the fluctuating shock waves is a major contributor to the unsteady pressure and form drag produced by the cavity.[4]

It is observed that for the Mach 1.8 and 2.1 cases, the cavity is generally spanned by two structures in the shear layer. This general observation may suggest that the second mode of oscillation is dominant at these Mach numbers. Zhang and Edwards[10] found the transition from longitudinal to transverse oscillation to occur near Mach 2.5 for cavities with a length-to-depth ratio of three. Therefore, the second mode is not as well defined for the two higher Mach number cases (2.8 and 3.5). This may further explain the suppression of large-scale structures at higher Mach numbers because transverse modes have been shown to gradually decrease the magnitude of the pressure fluctuation.[10]

Plan View Images

In addition to the streamwise views of the shear layer spanning the cavity, plan (x–z) views of the flowfield were taken for each freestream Mach number and are given in Fig. 5. These plan view images give insight into the three dimensionality of the flow. For the lower two Mach numbers (Figs. 5a and 5b), dark bands are seen running from the top to the bottom of each frame (spanwise in the tunnel). These bands indicate the entertainment of warmer fluid from the cavity into the shear layer in a highly two-dimensional fashion, spanning the full width of the cavity. This again suggests the presence of well-defined Brown and Roshko[17] roller-type structures. As indicated in the plan views, the structures become more three dimensional and less organized as the freestream Mach number is increased to 2.8 and particularly at Mach 3.5. This result has again been observed in compressible mixing layers[18–20] but is initiated at lower convective Mach numbers than seen here. Present in all of the plan view images are streamwise streaks, which have also been observed in planar mixing layers and are generally associated with the braid region.[20]

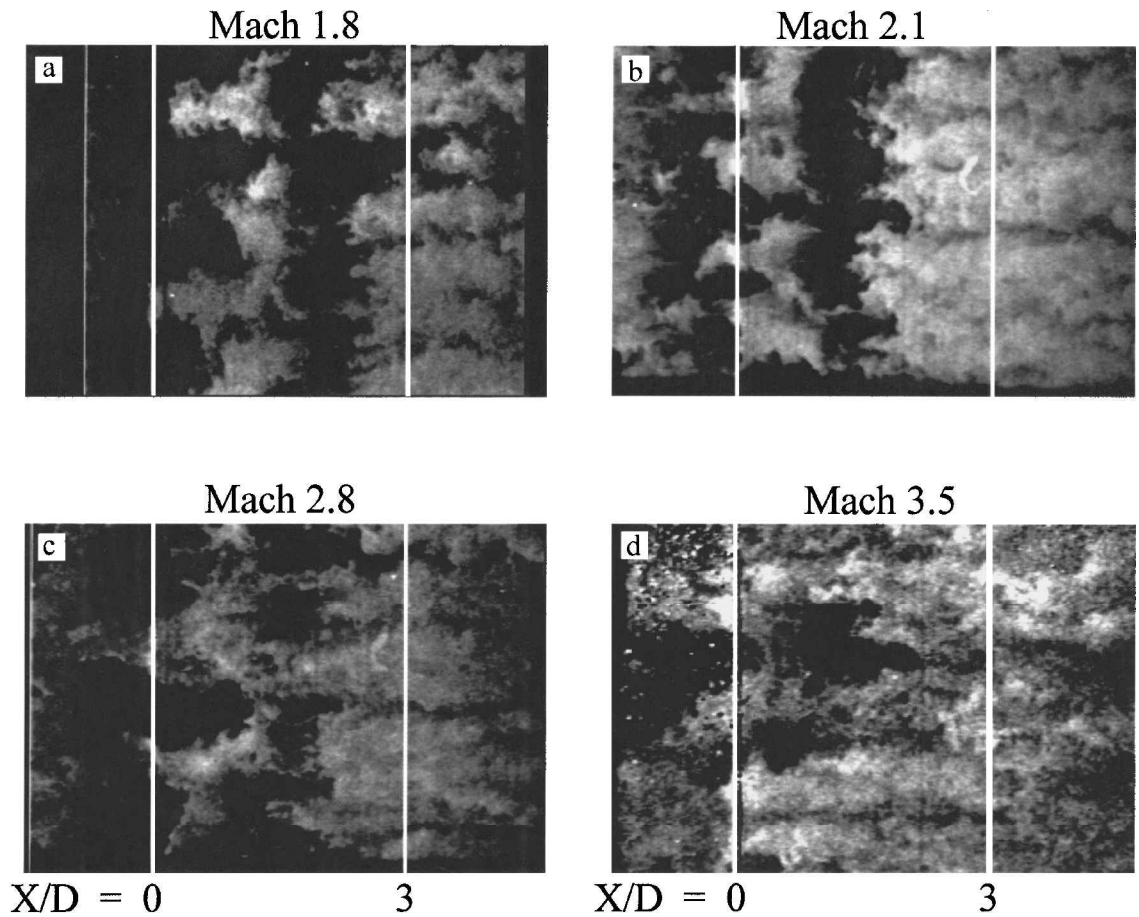

Fig. 5 Plan view images of flow over the cavity. The leading and trailing edges of the cavity are outlined in white, and the flow is moving from left to right.

Double-Pulse Images

Double-pulse imaging techniques are an excellent method for determining the velocity and evolution of large-scale structures in the shear layer. Using spatial correlation techniques (as described earlier) is advantageous in that it provides a statistical method without ambiguous interpretation. Image pairs of the flowfield over the cavity were obtained using the setup shown in Fig. 2. If the time delay between the images is short, or Taylor's frozen eddy hypothesis holds, the maximum of the correlation surface generated by an image pair will give the distance that the structures in the initial correlation window moved during the time delay. Therefore, the convective velocity can be calculated.

Figures 6–9 show initial and delayed streamwise (x–y) image pairs of the shear layer evolving over the two-dimensional cavity at Mach numbers of 1.8, 2.1, 2.8, and 3.5, respectively. Two instantaneous image pairs are given for each time delay and Mach number. Each image pair consists of an initial image (bottom) and a delayed image (top). Along with the cavity, the initial window and delayed correlation window corresponding to the maximum in the correlation surface in the delayed image are outlined in white.

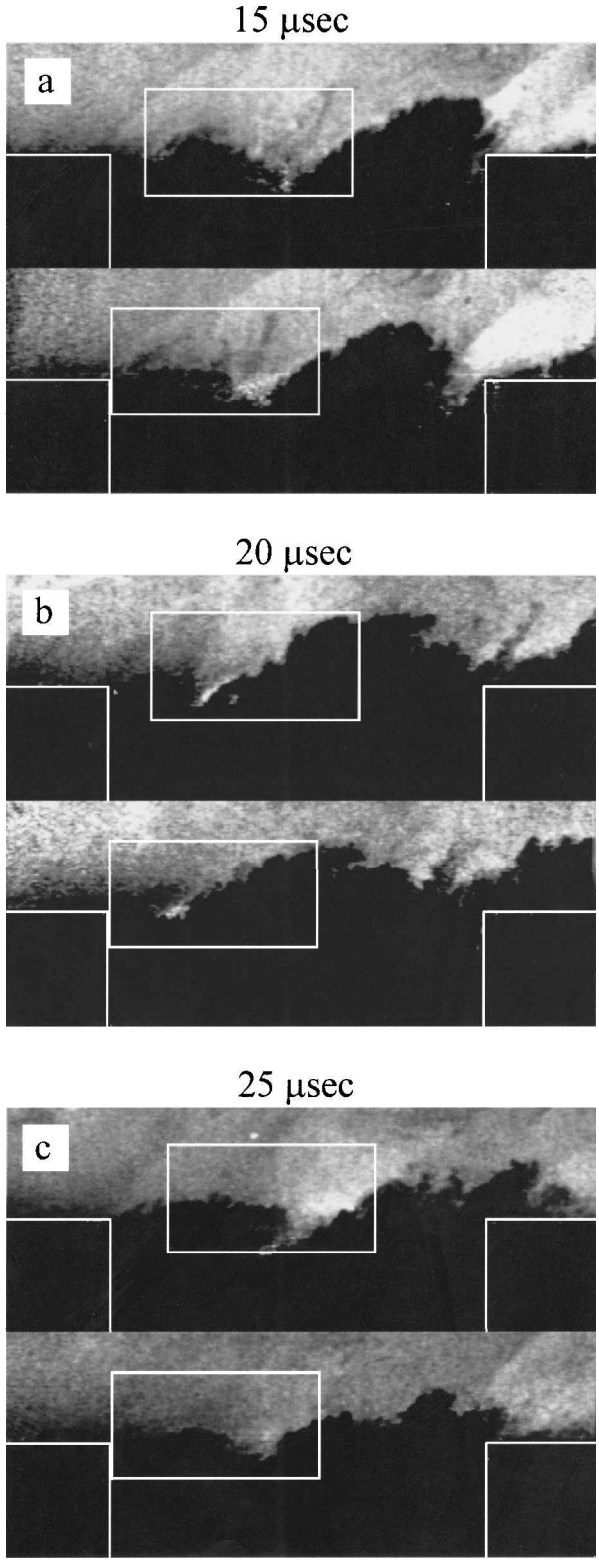

Fig. 6 Image pairs taken at Mach 1.8 using time delays of a) 15, b) 20, and c) 25 μs.

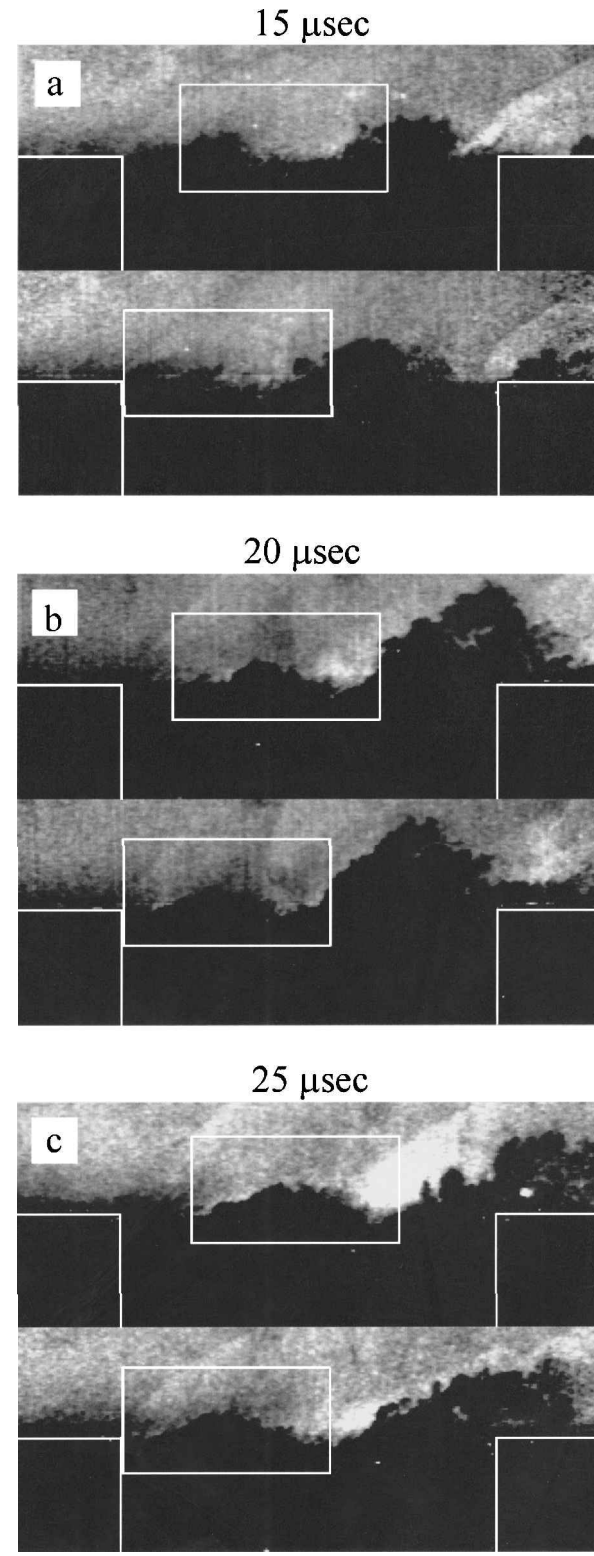

Fig. 7 Image pairs taken at Mach 2.1 using time delays of a) 15, b) 20, and c) 25 μs.

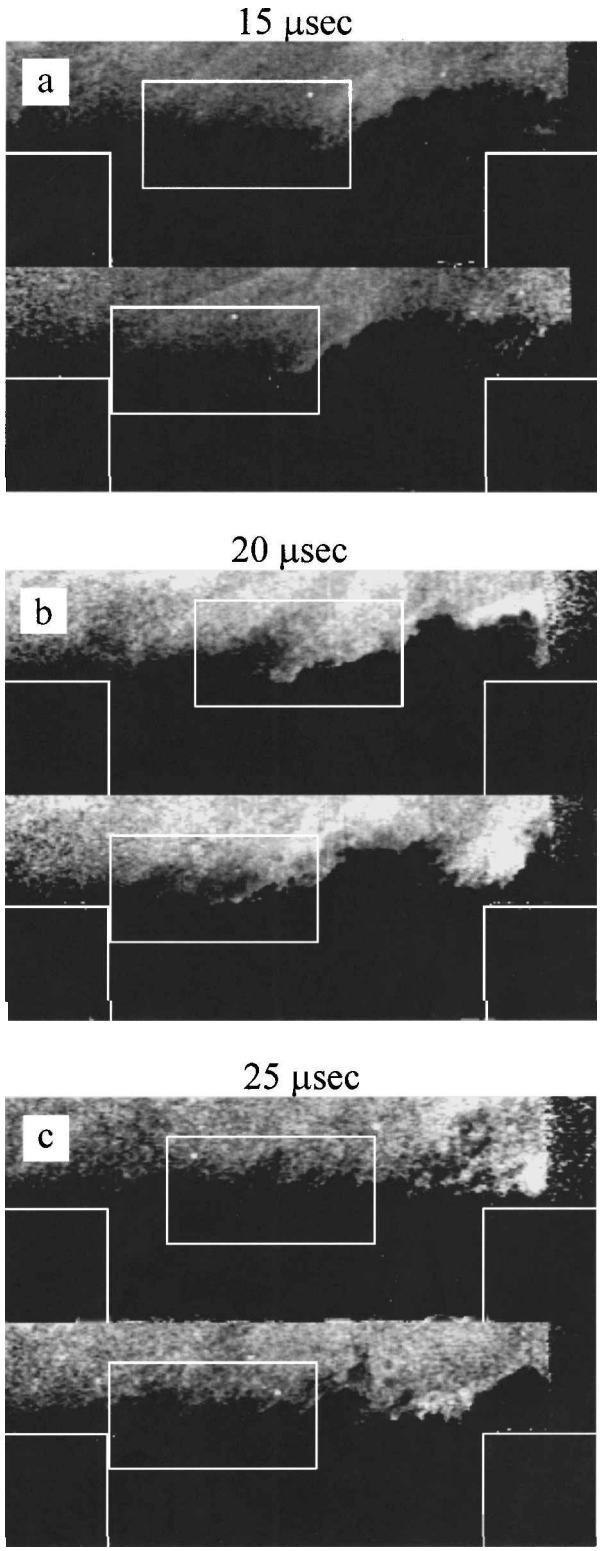

Fig. 8 Image pairs taken at Mach 2.8 using time delays of a) 15, b) 20, and c) 25 μs.

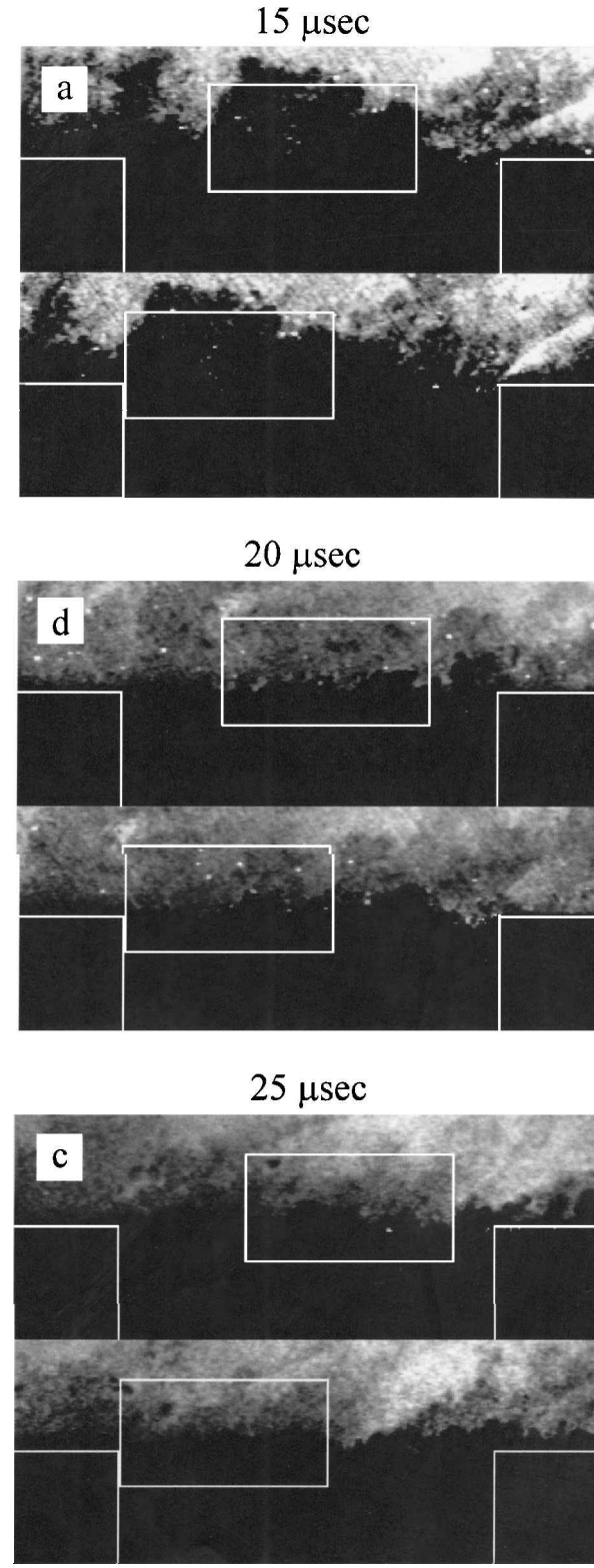

Fig. 9 Image pairs taken at Mach 3.5 using time delays of a) 15, b) 20, and c) 25 μs.

For all time delays in the Mach 1.8 case, large-scale roller-type structures are well defined and convect downstream without significant change in size or shape, even for the highest time delay. The distance traveled, of course, increases with the time delay but varies slightly for each instantaneous image within the given time delay. An interesting feature is seen in Fig. 6a. As the large-scale structure impinges on the trailing edge of the cavity, part of the structure is injected into the cavity and the trailing-edge shock changes shape as the structure convects and interacts with it. For the next time delay (Fig. 6b), the structure changes slightly, but still remains relatively coherent. These structures show little change as they pass over the trailing edge of the cavity. The structures interacting with the trailing-edge sometimes are stretched apart and sometimes pass over the cavity relatively unchanged. This is generally dependent on the lateral location of the structure within the cavity. The Mach 2.1 case (Fig. 7) shows essentially the same structure characteristics as outlined for the Mach 1.8 images.

Figure 8 shows initial and delayed images for a freestream Mach number of 2.8 above the cavity. At this Mach number the roller-type structures are still evident convecting downstream (Figs. 8a and

8b), but at other times are suppressed (Fig. 8c). When well-defined roller-type structures are evident, they remain identifiable for all time delays, but experience more significant changes in shape as the delay is increased. Images that show less coherent and smaller-scale structures are more difficult to follow from the initial to the delayed image, even with the help of the maximum correlation window. These characteristics will be quantified when correlation contours are calculated. Another characteristic suggested in a few of the images is the presence of shocks convecting with the large-scale structures (seen as faint discontinuities in intensity in the delayed correlation windows of Fig. 8b). These eddy shocklets have been suggested to be present for convective Mach number above unity in planar mixing layers, which is the case for the Mach 2.8 case.[13,14] They may be more prevalent than illustrated here, but may be masked by the quality of the images.

Examples of initial and delayed images are given in Fig. 9 for the Mach 3.5 case at the three time delays studied. As stated earlier few images show the well-defined, large-scale roller-type structures that are observed for the lower Mach number cases. Even when a more well-defined structure is evident (Fig. 9a), it does not have the roller-type characteristics observed earlier. For the higher two time delays, these less organized smaller-scale structures are not easily identifiable as they convect from the initial to the delayed image.

Correlation Surfaces

The resultant ensemble averaged correlation surfaces for the various Mach numbers and time delays are shown in Fig. 10. In each case, these surfaces were calculated with the initial correlation window in the location corresponding to the center of the shear layer and were made slightly larger than the largest structures found in the shear layer. In each plot, 15 contour levels were spaced from the maximum to minimum value. In general, the contours were found to be elliptical and inclined to the streamwise direction. The exception is the Mach 3.5 case where the correlation contours become more elongated as the time delay is increased. As the time delay is increased from 15 to 25 μs, the maximum correlation coefficient decreases for all of the Mach numbers by an average of 18%. To compare the decrease in the maximum correlation value between Mach numbers, it is necessary to compare the values at the same nondimensionalized time. This is given by

$$\tau = (\Delta t)\Delta U/\delta_{sl} \tag{6}$$

where Δt is the time delay, δ_{sl} is the visual shear layer thickness, and ΔU is the velocity difference across the shear layer (which is taken as the freestream velocity, assuming that flow is static in the cavity). To calculate the visual shear layer thickness, at the streamwise center of the cavity, 1125 instantaneous images were averaged together for each Mach number. The visual shear layer thickness is defined as the difference between the lateral location where the intensity was 10 and 90% of the freestream value (because the intensity goes to zero in the cavity). For Mach numbers of 2.1, 2.8, and 3.5, there was one time delay for each case where the nondimensionalized time τ was the same. These nondimensionalized times are given in Table 3 for each Mach number with the visual shear layer thickness, time delay, and maximum correlation level found. As the freestream Mach number increases from 2.1 to 3.5, the maximum correlation value

Table 3 Maximum cross-correlation values

M	t μs	δ_{sl} mm	τ	Peak cross correlation
2.1	15	6.8	1.87	0.66
2.8	20	6.2	1.89	0.64
3.5	25	5.0	1.89	0.51

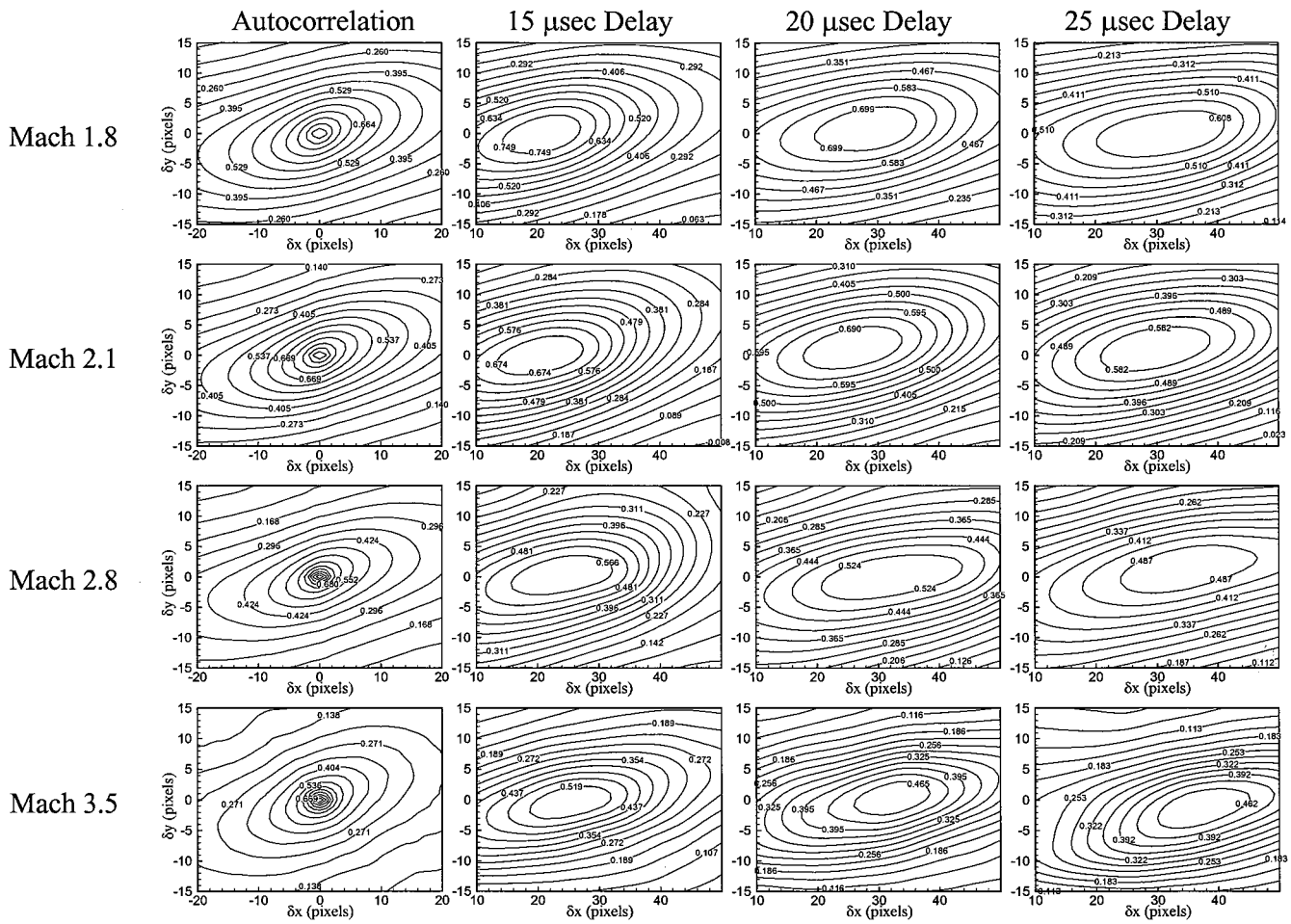

Fig. 10 Contour plots of correlation surfaces at each Mach number and time delay investigated. Each plot shows 15 contours of constant correlation, evenly distributed between the minimum and maximum value for that case.

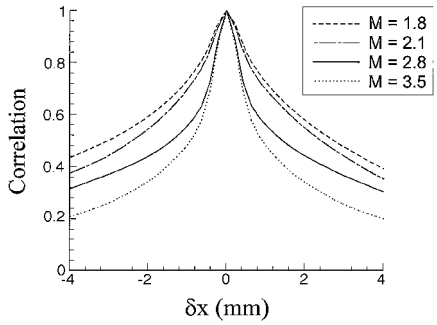

Fig. 11 One-dimensional slices of the autocorrelation surfaces taken at $\delta y = 0$ for various Mach numbers.

was found to decrease by 23%. This further supports the observation from the instantaneous images that the large-scale structures are less coherent, not as well defined (i.e., they do not have characteristics of roller-type structures), and may evolve more as the Mach number (and convective Mach number) is increased.

Autocorrelation

The autocorrelation may be viewed as the extrapolation of the correlations just given to zero time delay. Accordingly, they are placed to the left in Fig. 10. The autocorrelations can give useful information about the instantaneous characteristics of the large-scale structures in the shear layer. By definition, all of the autocorrelations have a peak correlation value of one. The contour levels of the autocorrelations show a much more distinct peak as the Mach number is increased. Figure 11 shows the $\delta y = 0$ slice of the autocorrelation peaks. It is clear from these plots that the peak of the autocorrelation function is much broader at the lower Mach numbers and steadily becomes sharper with increasing Mach number. This supports the conclusion that the structures are much larger and more coherent at the lower Mach numbers, requiring a larger shift to move them out of phase with themselves. At the higher Mach numbers, the structures are smaller and require only a small shift before they cease to overlap significantly and become uncorrelated. The full width at half maximum of the autocorrelation plots is, therefore, indicative of the average structure size in the correlation window. These were measured to be 5.8, 4.8, 2.8, and 1.8 mm for the Mach 1.8, 2.1, 2.8, and 3.5 cases, respectively. This corresponds to a monotonic decrease in structure size of 63% between Mach 1.8 and 3.5.

In all cases, the autocorrelations were elliptical in form and angled with respect to the freestream. Structure angles were approximated by fitting a line through individual isocontours given in Fig. 10. For all Mach numbers, the structure angle was found to increase from approximately 25 to 35 deg as the correlation level rose from 0.5 to 0.8 (where the number of points became too small). In planar mixing layers, structure angles have been reported to be approximately 20 deg, slightly decreasing with convective Mach number.[31]

Another structure characteristic, which can be calculated from the autocorrelation surfaces, is the eccentricity, defined as

$$e = \sqrt{1 - a/b}$$

where a is the width of the minor axis and b the width of the major axis. The eccentricity was also found to be a function of the correlation level. For the 0.5 correlation level, the eccentricity was found to be 0.75, 0.75, 0.66, and 0.62 for the Mach 1.8, 2.1, 2.8, and 3.5 cases, respectively. Thus, the average structure appears to become slightly more isotropic as Mach number is increased. In all cases, the eccentricity approached zero as the correlation level was increased.

Convective Velocity

To measure the convective velocity of the shear layer, the leading edge of the initial correlation window was placed 8 mm downstream from the leading edge of the cavity. This was done to give the shear layer structures some time to develop and correlate well. Changes in the size and position of the initial correlation window did not appear to have a significant effect on measured convective velocities. Because of the averaging process, the correlations should be dominated by large-scale shear layer structures, but because the correlation is also normalized by the standard deviation, smaller fluctuations can also have some contribution if they remain coherent over the time delay. As reported by other investigators, the convection velocity in compressible shear layers can vary across the thickness of the shear layer, from the high-speed side to the low-speed side.[19] Therefore, in the current study, the vertical position of the initial correlation window was varied laterally across the shear layer.

Uncertainties in the measured convective velocities can arise from several sources. Because they are so smooth and symmetric, locating the peak in the correlation surface to subpixel accuracy introduces little uncertainty (to do this a second-order polynomial was fit to the correlation peak and the surrounding nine points). However, the one-pixel uncertainty in camera alignment between the initial and delayed images was deemed to be much greater. This introduces an error ranging from 8 to 13 m/s into the velocity measurements as the time delay is increased from 15 to 25 μs. Another source of uncertainty is the change in the stagnation temperature, which was monitored and varies approximately 10 K between runs. This introduces an uncertainty in the velocity of less than 2% (from 6 to 8 m/s). Also, note that condensed particles that mark the shear layer structures may give some bias, but every effort was made to normalize the images and subtract the average so that form of the shear layer structure dominated the correlation. This procedure is discussed in detail by Murray.[23]

Figure 12 shows the convective velocity as measured with the initial correlation window at varying distances above and below the plane of the tunnel wall. The position of the window is based on the position of the center of the window. Some interesting trends appear to exist among the lateral convective velocity functions shown in Fig. 12. In each case, the convective velocity begins at some lower value on the cavity (lower speed) side of the shear layer, and, as the initial correlation window rises above the cavity floor, the measured convective velocity also rises, but levels off in the center of the shear layer. This is followed by a sharp increase to nearly the freestream velocity as the lateral position of the correlation window is increased. This may be interpreted as follows. When the initial correlation window is below the tunnel floor (in the cavity, $y < 0$) low-velocity structures on the cavity side of the shear layer structure are correlated. As the initial correlation window is moved upward into the vicinity of the shear layer (near $y = 0$), the larger structures in the shear layer will tend to dominate the correlation. This gives rise to the flat region most clearly seen in Figs. 12a–12c, where the measured convective velocity is nearly independent of the height of the initial correlation window over a relatively large distance. As the window moves farther up into the freestream, the smaller, less frequent disturbances in the freestream will occupy more of the correlation window and begin to dominate the correlation function. When this happens, the measured convective velocity then increases toward the freestream value. Another trend observed in the lateral profiles of Fig. 12 is that the convective velocity tends to decrease with increasing time delay. This is most likely due to the diminishing effects of the smaller-scale freestream turbulence structures on the correlation as the time delay increases.

Because the convective velocity varies laterally through the shear layer, the remaining challenge is to determine where to pick an average convective velocity representative of the large-scale structures in the shear layer for each case. The relatively flat region, which is presumed to be more representative of the large-scale structures in the shear layer, is the logical choice. From the approximate center of this flat region, convective velocities are plotted in Fig. 13. For all cases shown here, the $k_c = 0.57$ estimate appears to predict the experimentally determined values of U_c well and is within the scatter in the convective velocity measured for each time delay. The method proposed in Eq. (4), however, appears to overpredict the convective velocities in general. This bias is most likely due to the assumptions used in this equation that U_2 is approximately zero and that the temperature recovers in the cavity. Also, because the convective velocity is varying laterally, it is difficult to pick a single value at each Mach number, particularly at the highest Mach number studied (Mach 3.5).

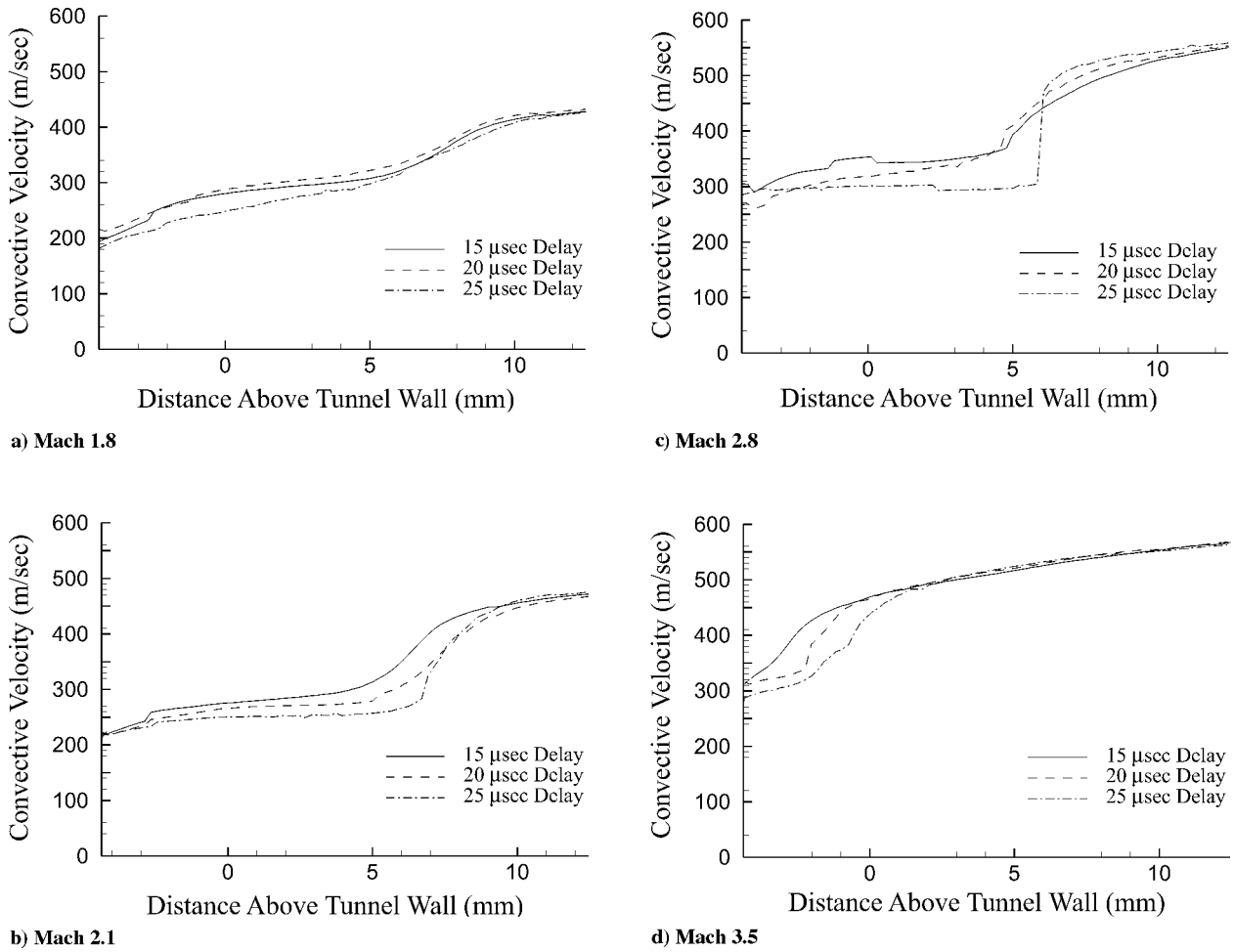

Fig. 12 Measured convective velocities shown as a function of the height of the initial correlation window above the tunnel wall. (Negative values are in the cavity.)

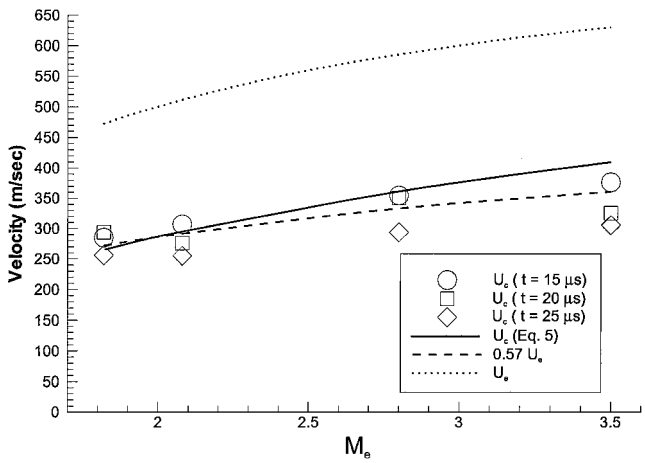

Fig. 13 Measured convective velocities from the "flat region" of Fig. 12 are plotted as a function of Mach number. Also plotted are the freestream velocity (U_e), the 0.57U_e estimate of U_c, and the estimate of U_c from Eq. (4).

Conclusions

The shear layer over a 3:1 rectangular cavity was investigated imaged using both schlieren and planer laser imaging techniques at Mach numbers of 1.8, 2.1, 2.8, and 3.5. This enabled the study and quantified (using correlation techniques) the shear layer large-scale structure characteristics over a range of compressibility levels. In the schlieren images, persistent leading- and trailing-edge shocks were seen, as well as a fluctuating shock with an associated shear layer structure. This fluctuating shock became less prevalent as the Mach number increased. Streamwise planar laser images show the shear layer to oscillate with large Brown and Roshko[17] roller-type structures at the lower Mach numbers. These structures become less prevalent as the Mach number is increased, although the cavity appears to cause the large two-dimensional structures to persist to higher levels of compressibility than in free shear layers. Plan view images also show two dimensionality to decrease with increasing Mach number. Autocorrelations performed on windows in the shear layer show the structure size to decrease greatly (63% from Mach 1.8 to 3.5) with increasing Mach number. With cross correlations between image pairs separated by 15-, 20-, and 25-μs delays, shear layer structures were tracked. For the same nondimensional time delay, the peak correlation level decreased by 23% as the Mach number was increased from 2.1 to 3.5. Measured convective velocities were found to vary laterally in the shear layer and were most accurately represented by 0.57 times the freestream velocity, which is generally used in Rossiter's[6] theory.

Acknowledgments

Gregory Elliott would like to acknowledge the support of the Air Force Office of Scientific Research for funding this work, the National Science Foundation for Grant NSF-9622108 with J. Foss, and the Air Force Research Laboratory with Mark Gruber. The authors would like to thank Doyle Knight for his assistance in interpreting these results and particularly for help in characterizing the state of the incoming boundary layer.

References

[1]Baysal, O., Fouladi, K., Leung, R. W., and Sheftic, J. S., "Interference Flows Past Cylinder–Fin–Sting–Cavity Assemblies," *Journal of Aircraft*, Vol. 29, No. 2, 1992, pp. 194–202.

[2]Asbury, S. C., Gunther, C. L., and Hunter, C. A., "Passive Cavity Concept for Improving the Off-Design Performance of Fixed-Geometry Exhaust Nozzles," AIAA Paper 96-2541, July 1996.

[3]Rockwell, D., and Naudascher, E., "Review—Self-Sustaining Oscillations of Flow Past Cavities," *Journal of Fluids Engineering*, Vol. 100, June 1978, pp. 152–165.

[4]Zhang, X., "Compressible Cavity Flow Oscillation Due to Shear Layer Instabilities and Pressure Feedback," *AIAA Journal*, Vol. 33, No. 8, 1995, pp. 1404–1411.

[5]Rizzetta, D. P., "Numerical Simulation of Supersonic Flow over a Three-Dimensional Cavity," *AIAA Journal*, Vol. 26, No. 7, 1988, pp. 799–807.

[6]Rossiter, J. E., "Wind Tunnel Experiments on the Flow over Rectangular Cavities at Subsonic and Transonic Speeds," British Aeronautical Research Council, Repts. and Memoranda 3488, London, Oct. 1964.

[7]Heller, H. H., and Bliss, D. B., "Physical Mechanism of Flow-Induced Pressure Fluctuations in Cavities and Concepts for Their Suppression," AIAA Paper 75-491, 1975.

[8]Ünalmis, O. H., Clemens, N. T., and Dolling, D. S., "Planar Laser Imaging of High-Speed Cavity Flow Dynamics," AIAA Paper 98-0776, 1998.

[9]McGregor, O. W., and White, R. A., "Drag of Rectangular Cavities in Supersonic and Transonic Flow Including the Effects of Cavity Resonance," *AIAA Journal*, Vol. 8, No. 11, 1970, pp. 1959–1964.

[10]Zhang, X., and Edwards, J. A., "An Investigation of Supersonic Oscillatory Cavity Flows Driven by Thick Shear Layers," *Aeronautical Journal*, Vol. 94, No. 940, 1990, pp. 355–364.

[11]Zhang, X., and Edwards, J. A., "Computational Analysis of Unsteady Supersonic Cavity Flows Driven by Thick Shear Layers," *Aeronautical Journal*, Vol. 92, No. 919, 1988, pp. 365–374.

[12]Papamoschou, D., and Roshko, A., "The Compressible Turbulent Mixing Layer: An Experimental Study," *Journal of Fluid Mechanics*, Vol. 197, 1988, pp. 453–477.

[13]Papamoschou, D., "Structure of the Compressible Turbulent Shear Layer," *AIAA Journal*, Vol. 29, No. 5, 1991, pp. 680, 681.

[14]Hall, J. L., Dimotakis, P. E., and Rosemann, H., "Experiments in Nonreacting Compressible Shear Layers," *AIAA Journal*, Vol. 31, No. 12, 1993, pp. 2247–2254.

[15]Elliott, G. S., and Samimy, M., "Compressibility Effects in Free Shear Layers," *Physics of Fluids A*, Vol. 2, No. 7, 1990, pp. 1231–1240.

[16]Goebel, S. G., and Dutton, J. C., "Experimental Study of Compressible Turbulent Mixing Layers," *AIAA Journal*, Vol. 29, No. 4, 1991, pp. 538–545.

[17]Brown, G. L., and Roshko, A., "On Density Effects and Large Structure in Turbulent Mixing Layers," *Journal of Fluid Mechanics*, Vol. 64, No. 4, 1974, pp. 775–816.

[18]Clemens, N. T., and Mungal, M. G., "Two- and Three-Dimensional Effects in the Supersonic Mixing Layer," *AIAA Journal*, Vol. 30, No. 4, 1992, pp. 973–981.

[19]Elliott, G. S., Samimy, M., and Arnette, S. A., "The Characteristics and Evolution of Large-Scale Structures in Compressible Mixing Layers," *Physics of Fluids*, Vol. 7, No. 4, 1995, pp. 864–876.

[20]Elliott, G. S., Samimy, M., and Arnette, S. A., "Study of Compressible Mixing Layers Using Filtered Rayleigh Scattering Based Visualization," *AIAA Journal*, Vol. 30, No. 10, 1992, pp. 2567–2569.

[21]Plentovich, E. B., Stallings, R. L., Jr., and Tracy, M. B., "Experimental Cavity Pressure Measurements at Subsonic and Transonic Speeds," NASA TP 3358, Nov. 1993.

[22]Ünalmis, Ö. H., Clemens, N. T., and Dolling, D. S., "Planar Laser Imaging of a Supersonic Side-Facing Cavity," AIAA Paper 99-0297, 1999.

[23]Murray, R. C., "A Study of the Shear Layer over a Two-Dimensional Cavity Using Correlation Techniques," M.S. Thesis, Dept. of Mechanical and Aerospace Engineering, Rutgers Univ., Piscataway, NJ, May 1999.

[24]Samimy, M., and Lele, S. K., "Motion of Particles with Inertia in a Compressible Free Shear Layer," *Physics of Fluids*, Vol. 3, No. 8, 1991, pp. 1915–1923.

[25]Smith, D. R., "The Effects of Successive Distortions on a Turbulent Boundary Layer in a Supersonic Flow," Ph.D. Dissertation, Dept. of Mechanical and Aerospace Engineering, Princeton Univ. Princeton, NJ, Jan. 1993.

[26]Samimy, M., "An Experimental Study of Compressible Turbulent Reattaching Free Shear Layers," Ph.D. Dissertation, Dept. of Mechanical and Industrial Engineering, Univ. of Illinois, Urbana, IL, 1984.

[27]Hopkins, E. J., and Inouye, M., "Evaluation of Theories for Predicting Turbulent Skin Friction and Heat Transfer on Flat Plates at Supersonic and Hypersonic Mach Numbers," *AIAA Journal*, Vol. 9, No. 6, 1971, pp. 993–1003.

[28]Heller, H., and Delfs, J., "Cavity Pressure Oscillations: The Generating Mechanism Visualized," *Journal of Sound and Vibration*, Vol. 196, No. 2, 1996, pp. 248–252.

[29]Zhang, X., Rona, A., and Edwards, J. A., "An Observation of Pressure Waves Around a Shallow Cavity," *Journal of Sound and Vibration*, Vol. 214, No. 4, 1998, pp. 771–778.

[30]Miles, R. B., and Lempert, W., "Two-Dimensional Measurement of Density, Velocity, and Temperature in Turbulent High-Speed Flows by UV Rayleigh Scattering," *Journal of Applied Physics*, Vol. 51, No. 1, 1991, pp. 1–7.

[31]Messersmith, N. L., Dutton, J. C., and Krier, H., "Engineering Investigation of Large-Scale Structures in Compressible Mixing Layers," AIAA Paper 91-0244, Jan. 1991.

[32]Smith, K. M., and Dutton, J. C., "A Procedure for Turbulent Structure Convective Velocity Measurements Using Time-Correlated Images," *Experiments in Fluids*, Vol. 27, No. 3, 1999, pp. 244–250.

M. Samimy
Associate Editor